Available online at www.sciencedirect.com
ScienceDirect
Journal of the European Ceramic Society 31 (2011) 1361–1369
www.elsevier.com/locate/jeurceramsoc

Influence of porosity on the mechanical properties of microporous β-TCP bioceramics by usual and instrumented Vickers microindentation

A. Tricoteaux [a,b,*], E. Rguiti [a,b], D. Chicot [a,c], L. Boilet [a,b], M. Descamps [a,b], A. Leriche [a,b], J. Lesage [a,c]

[a] *Univ Lille Nord de France, F-59000 Lille, France*
[b] *UVHC, LMCPA, F-59600 Maubeuge, France*
[c] *USTL, LML, F-59650 Villeneuve d'Ascq, France*

Received 6 October 2010; received in revised form 17 January 2011; accepted 3 February 2011
Available online 26 February 2011

Abstract

Beta-tricalcium phosphate [$Ca_3(PO_4)_2$, β-TCP] is a bioresorbable material showing an excellent biocompatibility. However, sintering of β-TCP is difficult and the material presents poor mechanical strength and a low resistance to crack-growth propagation. In this study, influence of the porosity on the hardness and the elastic modulus is studied by means of usual and instrumented microindentation tests. Nevertheless, indentation diagonals measurement by optical observations is not accurate due to the crack formation around the residual indent. That is why instrumented indentation test which allows deducing the hardness and the bulk modulus from the load–depth curve analysis is used as an alternative method. The corresponding hardness number can be calculated by using the maximum indentation depth (Martens Hardness) or the contact depth determined by Oliver and Pharr's method (Contact Hardness). But in order to give representative values when comparing classical and instrumented hardness measurements, Martens hardness is preferred because its value can be directly related to the value of the Vickers hardness number by simple geometrical considerations.

In this work, bioceramics were produced by conventional sintering of β-TCP powders synthesized by aqueous precipitation. Different process conditions were chosen to obtain microporous ceramics with a porosity rate between 0 and 14% in volume. As main results, the elastic modulus is found decreasing between 166 GPa and 108 GPa and the hardness number from 4.4 GPa to 2.2 GPa when increasing the porosity rate. A model connecting mechanical properties to porosity rate and grain arrangement is validated for the elastic modulus whereas deviation is observed for the hardness number. However, we propose an original approach where the relative variation of the two mechanical properties can be expressed with a unique relation as a function of the porosity volume fraction.

Keywords: β-TCP; Biomedical applications; Porosity; Mechanical properties; Instrumented microindentation

1. Introduction

Bioceramics based on calcium phosphate, mainly hydroxyapatite (HA) and β tricalcium phosphate (β-TCP), are currently employed for bone substitute applications.[1–4] These materials exhibit a chemical composition very close to that of a bone, an excellent biocompatibility and very interesting osteoconduction properties. However, β-TCP shows much more significant bioresorption after implantation than the HA, which is poorly resorbable. Thus, β-TCP material is easily replaced by the newly formed bone.[5] This enables the use of increasingly frequent β-TCP for these clinical applications at the expense of the HA and classical biphasic HA/β-TCP. In addition to their functionality of filling bone, these materials can be used as a biological agent reservoir for prophylactic or therapeutic functions. These ceramics can be charged with drugs such as growth factors, anticancer drugs or antibiotic agents which are gradually released in the implantation site.[6–8] The storage of these active agents in ceramics requires the development of microporosity inside the bone substitute. Moreover, this microporosity is benefit to cellular response[9] or to the resorption kinetics change of the material.[10] For such applications, it is necessary studying the influence of the porosity on the mechanical properties of the β-TCP.

* Corresponding author at: UVHC, LMCPA, F-59600 Maubeuge, France.
E-mail address: Arnaud.Tricoteaux@univ-valenciennes.fr (A. Tricoteaux).

0955-2219/$ – see front matter © 2011 Elsevier Ltd. All rights reserved.
doi:10.1016/j.jeurceramsoc.2011.02.005

Among the experimental methods for determining the mechanical properties of ceramics, the indentation test presents some interesting advantages.[11] The mechanical properties determination by indentation can be performed by usual indentation tests consisting in geometrical analysis of the residual indent or by load–depth curve analysis obtained by instrumented indentation. For standard Vickers indentations applied to brittle ceramics, cracks are often generated along the indent diagonals. As a consequence, the presence of these cracks can have influence on the diagonal lengths measurement. Mainly for this reason, load–depth curve analysis is preferred for calculating mechanical properties since their determination results from indentation depth measurement which is not affected by the cracking network. That is why to circumvent this experimental problem some authors have used instrumented nanoindentation to characterize single crystals of hydroxyapatite and tricalcium phosphate bioceramics.[12–15] In addition, a large discrepancy of results, depending on the material behaviour and the indentation testing conditions, were observed in literature. As an example, processing parameters such as sintering temperature, porosity, and grain size can influence the indentation response. Furthermore, applied load, indenter geometry and hold-time can also modify the value of the mechanical properties depending on the indentation size effect and the visco-elastoplastic behaviour of the material. Moreover, the hardness number greatly varies according to the hardness calculation (Vickers, Meyer, Martens, Oliver and Pharr, etc.). Additionally, the deformation of the instrument/specimen couple and the rounding tip effect must be taken into account depending on the scale of measurement (nano or micro). Consequently, we found in literature hardness values ranging between 0.6 GPa and 7.7 GPa and Young's modulus between 24 GPa and 121 GPa where the highest values are obtained for dense single crystal of β-TCP ceramics.[14]

To reduce such a discrepancy, we suggest studying the effect of porosity by means of complementary methods, i.e. usual and instrumented indentation. The elastic modulus is determined by Vickers instrumented indentation when the frame compliance of the instrument/specimen system is explicitly taken into account. Additionally, usual Vickers hardness and instrumented Martens hardness are compared for subtracting the crack influence on the hardness number. The macrohardness associated to the hardness length-scale factor are also analyzed. Finally the mechanical properties are studied as a function of the porosity of β-TCP microporous ceramics.[16]

2. Experimental

2.1. β-TCP microporous ceramics

2.1.1. Synthesis and characterisation of β-TCP powder

β-Tricalcium phosphate powders were synthesized by co-precipitation of a mixture of diammonium phosphate $NH_4(HPO_4)_2$ (Carlo Erba, France) and calcium nitrate $Ca(NO_3)_2{\cdot}4H_2O$ (Brenntag, France) using aqueous precipitation technique. Ca/P ratio is chosen equal to 1.52 according to recent work at the laboratory.[17] For these conditions, a stoichiometric powder is obtained as shown on XRD patterns and FTIR spectra (Fig. 1). Indeed, X-ray diffraction analysis indicates a well-crystallized powder, which can be indexed by the β-TCP diagram (ICDD n°01-070-2065) (Fig. 1a). Moreover, the main peak of HA (diffraction plane (2 1 1) at $2\theta = 31.7°$) is not observed. Except the peaks at 3460 and 1650 cm^{-1} (that can be attributed to adsorbed H_2O and CO_2), all the bands in the FTIR spectra (Fig. 1b) correspond to PO_4^{3-} groups (stretching modes between 900 and 1130 cm^{-1} and bending modes between 550 and 600 cm^{-1}). The characteristic bands of calcium pyrophosphate at 723, 1185 and 1210 cm^{-1} are not observed due to a defect in calcium.

The pH of the solution was maintained constant at 6.4 during the reaction by a continuous ammonia addition. The temperature was fixed at 30 °C and maturation was carried out during 24 h. After ripening, the solution was filtered and the precipitate dried at 80 °C. The as-obtained powder exhibit high specific surface area (>60 $m^2\ g^{-1}$) for the proposed shaping process. As a consequence, the precipitate was calcined at high temperatures for increasing the average primary particle size. Different calcination temperatures were used to obtain powder batches with various grain characteristics. Afterwards, β-TCP was crushed in order to break agglomerates formed during calcination for obtaining the smallest powder size. This process was performed by ball milling during 5 h in High Density Poly Ethylene (HDPE) milling jars with yttrium stabilized zirconia balls.

2.1.2. Slip preparation and thermal treatment

β-TCP slurries with 65 wt.% of dry matter were prepared with distilled water. The slurry dispersion was ensured by adding 1.5 wt.% of commercial organic dispersant (Darvan C, R.t. Vanderbilt. Co.) and ball milling during 1 h. Cylindrical specimens (20 mm diameter – 5 mm height) were elaborated by slip casting. After drying, the specimens were naturally sintered where the processing parameters such as calcination temperature, sintering temperature and duration have been adapted for obtaining various densities and similar grain sizes (Table 1). Density and opened porosity of the sintered samples were measured by hydrostatic weight method considering the β-TCP theoretical density equals to 3.07 $g\,cm^{-3}$. The mean TCP grain size was calculated with a mean linear intercept method. After sintering, some samples have undergone a post-HIP treatment at 1050 °C under 150 MPa and Ar/O_2 atmosphere to obtain maximum density. The HIP treatment was carried out on samples initially sintered at 1060 °C for 2 h presenting a close density up to 98% of the theoretical full dense β-TCP. After this treatment, the sample obtained a relative density equal to 100% and showed a semi-transparent appearance. The ceramic translucency confirms the absence of micropores which absorb and scatter the light.

2.2. Indentation experiments

Instrumented indentation experiments were carried out with a micro-hardness CSM 2-107 Tester equipped with a Vickers diamond indenter at maximum loads chosen within the range

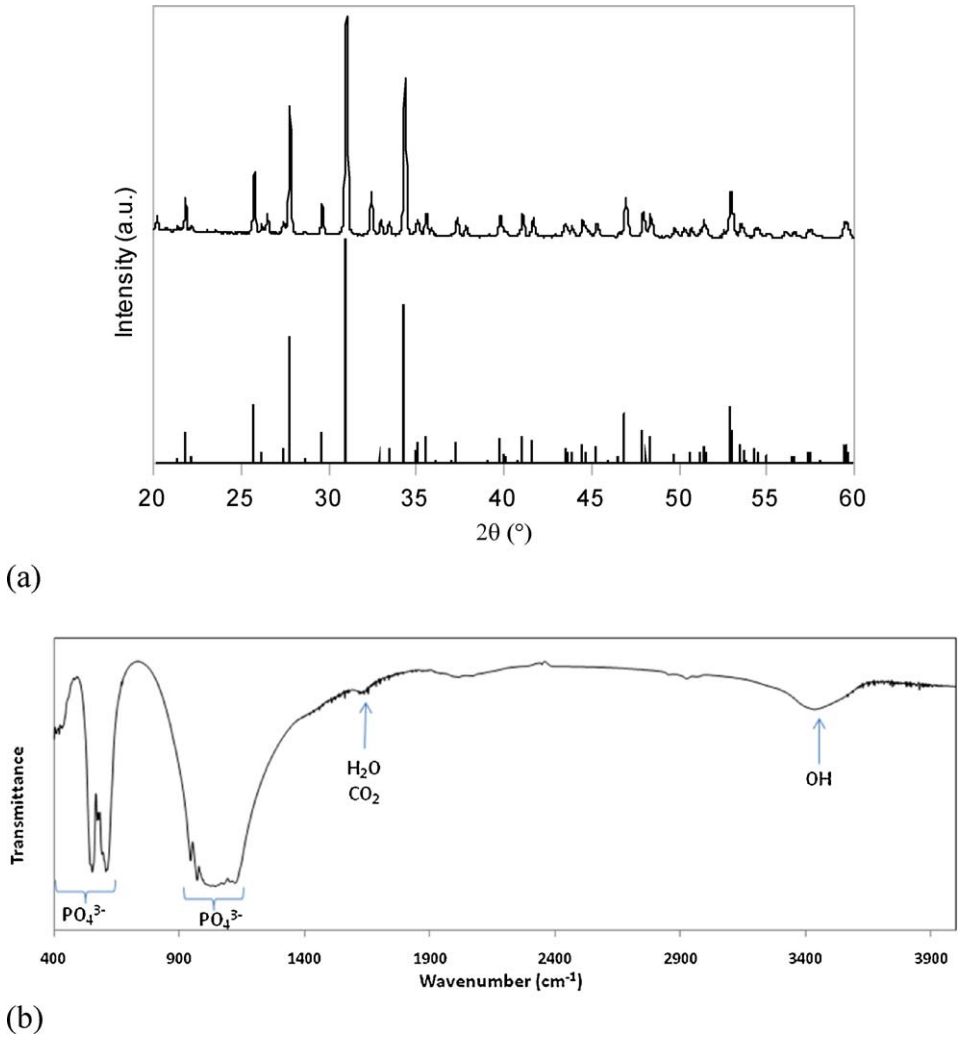

Fig. 1. XRD pattern (compared with the ICDD n°01-070-2065) (a) and IR spectrum (b) of the synthesized β-TCP powder.

40–2000 mN. Three tests were performed for each applied load. The values of the loading and unloading rates (expressed in mN/min) were set up in order to achieve the maximum applied loads in 30 s independently on its value. As an example, when the maximum load equals to 1000 mN, the loading and unloading rates are equals to 2000 mN/min. A hold-time of 15 s is imposed according to the standard CSM test procedure in order to partially avoiding the artefacts related on the creep and the filling of porosities. Standard Vickers indentation tests were performed with a micro-indenter under loads ranging from 250 to 5000 mN and a hold-time of 15 s under the maximum load. Each specimen was indented three times at each applied load.

3. Mechanical properties determination by indentation: theoretical background

Instrumented indentation test is largely used to determine elastic modulus and hardness of massive materials since it is a relevant and non-destructive method. During an indentation test, the applied load, P, is plotted as a function of the indenter displacement, h. The elastic modulus, E, and the hardness, H, is then calculated from the analysis of the unloading part of the indentation (P–h) curve which is schematically represented in Fig. 2.

For calculating the mechanical properties, different approaches and/or hypotheses can be implemented and the

Table 1
Processing parameters and microstructure characteristics of microporous ceramics.

Calcination temperature (°C)	Sintering temperature (°C)	Sintering duration (h)	Relative density (%)	Open/close porosity (%)	Grain size (μm)
900	1000	5	86	12.7/1.3	0.85 ± 0.08
900	1040	2	89	9.5/1.5	0.86 ± 0.07
750	1040	2	95	0.3/4.7	1.03 ± 0.13
750	1060	2	98	0.1/1.9	1.17 ± 0.13

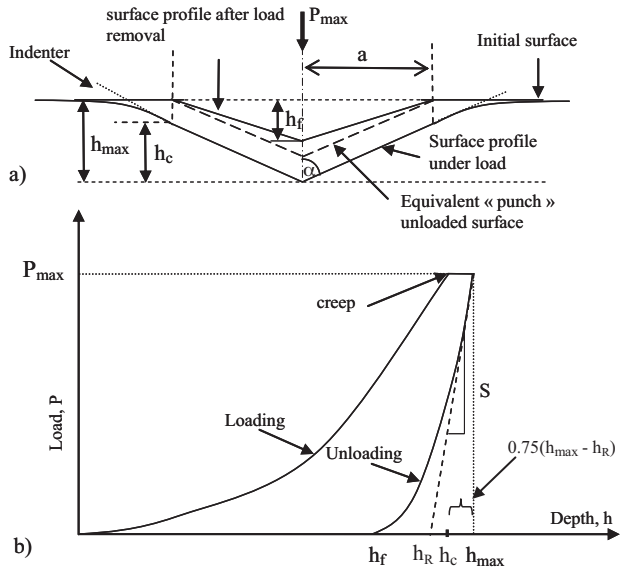

Fig. 2. (a) Schematic cross-section of a conical indent and (b) a load–depth curve and the corresponding indentation depths used to calculate hardness numbers.

results can be modified. That is why it is necessary to well-specify the methodology employed for the indentation depth measurements and the expressions allowing calculating the different parameters, in particular by considering or not the frame compliance.

Indeed several indentation depths are defined: h_{max} is the maximum indentation depth reached by the indenter during the indentation test, h_f is the final indentation depth, h_R is the residual indentation depth resulting from the slope of the unloading curve calculated at P_{max} and h_c is the contact depth defined by Oliver and Pharr[18] to take into account the deformation around the indent. For Vickers indentation, h_c is calculated from h_{max} for which 0.75 $(h_{max} - h_R)$ is subtracted.

3.1. Elastic modulus

Oliver and Pharr[18] suggest calculating the elastic modulus on the base of Sneddon's analysis[19] describing the contact between a rigid conical indenter and an elastic semi-infinite half-space. The authors propose to determine the reduced modulus E_R as a function of the indentation parameters deduced from the unloading part of the load–depth curve (Fig. 2).

$$E_R = \frac{1}{2}\left(\frac{dP}{dh}\right)_{h_{max}} \frac{\sqrt{\pi}}{\sqrt{A_p}} \quad (1)$$

where dP/dh is the slope of the unloading curve representing the contact stiffness, A_p is the projected contact area and E_R is defined as:

$$\frac{1}{E_R} = \frac{1-\nu^2}{E} + \frac{1-\nu_i^2}{E_i} \quad (2)$$

where E, ν and E_i, ν_i represent the Young's modulus and Poisson's ratio of the material and the indenter respectively.

Relation (1) is related to theoretical analysis of conical, spherical and flat indenters. But authors showed that two correction factors must be introduced to take into account the specific shape of the indenter[20–22] and the radial displacements of the semi-infinite half space into the contact circle area during indentation.[23] Then a shape factor, β, linked to the indenter geometry is introduced in Eq. (1). For a Vickers indenter, King[20] proposed a value of 0.012 for β, whereas Dao et al.[21] proposed a value of 1.07. Finally, a three dimensions simulation leads to $\beta = 1.05$, which is material independent.[22] On the other hand, Hay et al.[23] introduced a correction factor, γ, which only depends on Poisson's coefficient:

$$\gamma = \pi \frac{(\pi/4) + 0.1548((1-2\nu)/4(1-\nu))\cot\Psi}{(\pi/2) + 0.8312((1-2\nu)/4(1-\nu))\cot\Psi} \quad (3)$$

where Ψ represents the half-angle of the equivalent conical indenter which would produce the same contact area of a Vickers indenter under the same load. It is equal to 70.3°. ν is the Poisson's ratio of the tested material.

Finally, relation (1) must be applied as follows:

$$E_R = \frac{1}{2(\beta\gamma)}\left(\frac{dP}{dh}\right)_{h_{max}} \frac{\sqrt{\pi}}{\sqrt{A_p}} \quad (4)$$

In order to validly apply relation (4), two problems linked to the projected contact area calculation and the slope of the unloading curve must be solved. In microindentation, the rounded tip effect can be neglected due to the very lower tip defect length in comparison to the indentation depth. Then, the projected contact area is calculated from geometrical considerations of the Vickers indenter shape by:

$$A_p = 24.5h_c^2 \quad (5)$$

where h_c is the contact indentation depth calculated by following the methodology of Oliver and Pharr.[18]

During instrumented indentation test with a conical indenter, the unloading response is not fully linear contrary to that observed for a flat "punch" indenter. Assuming equivalent conical indenter behaviour at the beginning of the unloading curve, Oliver and Pharr calculate the contact indentation depth h_c from the contact stiffness dP/dh calculated at h_{max}. Afterwards, Oliver and Pharr suggested describing the unloading curve by a power law as follows:

$$P = B(h - h_f)^m \quad (6)$$

where B, h_f and m are material constants determined by fitting the experimental data.

In order to avoid possible artefacts on the unloading curve, i.e. the "bowing-out" at the maximum load and the "comma" before the complete withdrawal of the indenter, only data ranging between 40% and 98% of the maximum load are considered for the fitting. The choice of these values is discussed by Chicot et al.[24] After calculation, the contact stiffness is then equal to:

$$\left(\frac{dp}{dh}\right)_{h_{max}} = S_u = mB(h_{max} - h_f)^{m-1} \quad (7)$$

which allows calculating the contact indentation depth, h_c, according to the methodology of Oliver and Pharr:

$$h_c = h_{max} - \varepsilon \frac{p_{max}}{S_u} \quad (8)$$

where ε is equal to 0.75 for Vickers indenter.

However, application of relation (4) requires the contact stiffness calculation, i.e. (dP/dh). During the indentation test, the displacement which is given by the instrument both depends on the penetration depth of the indenter into the material and on the elastic deformation of the instrument. To separate these two contributions, Fischer-Cripps[25] considers that the indenter/specimen and the instrument frame can be assimilated to two springs associated in series. As a result, the total compliance is the sum of the frame compliance, C_f, and the indenter/specimen, C_s. Then, by combining the relations (4) and (5), we can write relation (9) since the compliance corresponds to the inverse of the contact stiffness:

$$C = \left(\frac{dh}{dP}\right)_{h_{max}} = C_f + \frac{1}{2(\beta\gamma)}\sqrt{\frac{\pi}{10.5}}\frac{1}{E_R}\frac{1}{h_c} \quad (9)$$

which allows to calculate the reduced modulus from the slope of the straight line representing the inverse of the contact stiffness as a function of the inverse of the contact indentation depth.

3.2. Hardness

The hardness of a material represents its resistance to plastic deformation under indentation. The general relation for calculating a hardness number is given by:

$$H = \frac{P}{A} \quad (10)$$

where H is the hardness number, P the applied load and A is the area of the indent.

For usual indentation tests, the hardness number can be calculated by considering the actual or the projected contact area. The different calculations are summarized in Table 2. For a Vickers indenter, the actual contact area is used to calculate the Vickers hardness number whereas the Meyer hardness number is obtained by considering the projected contact area. In addition for instrumented indentation, the contact indentation depth is used to calculate the contact hardness number following the Oliver and Pharr methodology. On the other hand, the Martens hardness number takes into account the maximum indentation depth.

In order to validly compare usual and instrumented indentation results, it is more convenient to calculate Vickers (HV) and Martens (HM) hardness numbers because simple geometrical considerations of the pyramid dimensions allows connecting the indent diagonal to the maximum indentation depth by a factor 7. As a consequence by using this proportionality ratio, HV becomes mathematically equal to HM.

On the other hand, sharp indentations of very brittle materials such as ceramics can generate cracks along the diagonals and/or in the region of the indent. The presence of cracks can impede accurate optical measurements of the indent diagonal length. In addition, the visco-elastic recovery occurring during the unloading may also influence the geometry of the residual indent. Then, usual hardness calculation can lead to different values compared to Martens hardness; that is the reason why we applied the two hardness calculations.

However, the hardness number is load-dependent resulting from the Indentation Size Effect (ISE). This phenomenon has been associated with various causes such as work hardening, roughness, piling-up, sinking-in, shape of the indenter, surface energy, varying composition and crystal anisotropy, which have been all discussed extensively by Cheng and Cheng.[26] In the case of ceramics, Gong et al.[27] attribute the ISE to micro-cracking around and under the indenter whereas Peng et al.[28] link the ISE to the elastic recovery occurring after the indenter withdrawal. Many relationships have been suggested for describing this hardness-load dependence by expressing the applied load, P, as a function of the indent diagonal, d, or the hardness, H, as a function of the indentation depth, h.[29]

By analysing experimental hardness results, the majority of these relations are able to adequately represent the hardness-load dependence from a mathematical point of view. However when studying ISE in nano and in microindentation, it is observed that the fitting or the theoretical parameters involved in these models change without any clear justifications. In order to explain this difference and to conciliate nano and microindentation results, Chicot[16] suggests the use of the hardness length-scale factor based on the strain gradient plasticity theory proposed by Nix and Gao.[30]

$$H_{LSF} = H_0\sqrt{h^*} \quad \text{when} \quad H^2 = H_0^2 + \frac{H_{LSF}^2}{h} \quad (11)$$

where H_0 corresponds to the macrohardness that would be obtained for an infinite applied load and h^* is a characteristic length that represents the ISE. H_{LSF} is the hardness length-scale factor equivalent to a deformation toughness since it is expressed in MPa $m^{1/2}$. This parameter is used to represent the plastic deformation behaviour of the material under the indent.

4. Results and discussion

4.1. Elastic modulus

According to relation (9), we plotted in Fig. 3 the inverse of the contact stiffness, $1/S = (dh/dP)h_{max}$, as a function of the reciprocal indentation depth, $1/h_c$. Fig. 3 clearly shows that the variations can be represented by a straight line which intercepts the y-axis at different values corresponding to the frame compliance. This result is very important since it validates the methodology considering no fixed value for the frame compliance before the indentation test. In fact, a given value for C_f will lead inevitably to a wrong value for the corresponding slope.

Then, we calculated the elastic modulus from the slope of the straight lines by applying the methodology described in Section 3.1. The correction factor introduced by Hay et al.[23] involves the Poisson's ratio of the tested material. By considering a value of 0.3 for the β-TCP Poisson's ratio, γ is then equal to 1.067. Afterwards, to calculate the elastic modulus, the elastic proper-

Table 2
Hardness number calculations considering actual or projected contact areas and different indentation depths.

Contact area	Usual indentation	Instrumented indentation	
	Indent diagonal	Maximum indentation depth	Contact indentation depth
Actual	$HV = 1.8544\frac{P}{d^2}$ Vickers hardness	$HM = \frac{P}{26.43h_{max}^2}$ Martens hardness	$H = \frac{P}{26.43h_c^2}$
Projected	$HMe = 2\frac{P}{d^2}$ Meyer hardness	$H = \frac{P}{24.5h_{max}^2}$	$HIT = \frac{P}{24.5h_c^2}$ Contact hardness

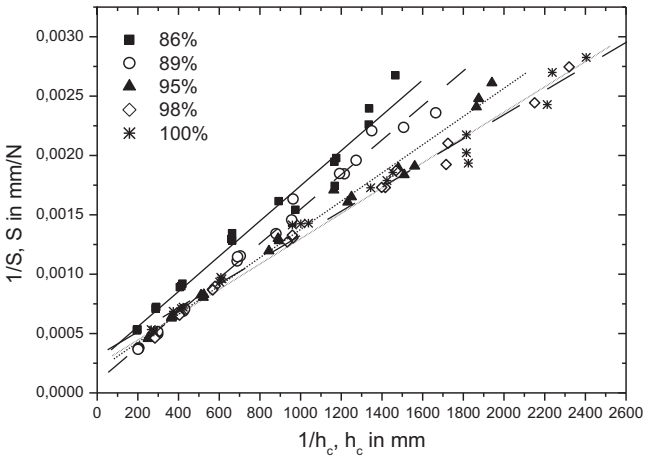

Fig. 3. Inverse of the contact stiffness as a function of the inverse of the contact indentation depth according to the porosity rate.

ties of the diamond are 0.007 and 1140 GPa for the Poisson's ratio and the elastic modulus, respectively.[31] Table 3 collects the different values for the elastic modulus calculated for the microporous β-TCP ceramics according to the porosity volume fraction.

As shown in Table 3, the elastic modulus increases from 108.2 GPa to 165.9 GPa when the ceramic density increases from 86% to 100%. To study the influence of the porosity on the elastic modulus, we applied the model of Jernot et al.[32] previously developed for sintered materials. This model earlier modified by Tancret et al.[33] was applied to micro and macro porous β-TCP ceramics. In the case of microporous ceramics for which the pore lengths are less than 1 μm, the mathematical expression is reduced to:

$$E = E_0[N_C(1-p) - (N_C - 1)(1-p)^{2/3}] \quad (12)$$

where E_0 is the Young's modulus of the dense ceramic, p the porosity volume fraction and N_C the mean coordinate number, i.e. the number of neighbours for each grain.

Table 3
Elastic modulus obtained by instrumented indentation performed on microporous β-TCP ceramics according to the porosity rate.

Density	E (GPa)	Error (GPa)	R^2
86%	108.2	±4.6	0.98765
89%	110.6	±2.5	0.99583
95%	138.6	±3.3	0.99552
98%	156.9	±3.5	0.99663
100%	165.9	±5.3	0.99253

Fig. 4 represents the application of relation (12) to the β-TCP microporous ceramics. The R-square value is relatively high, i.e. 0.975, allowing validating the model. The values of E_0 and N_C correspond to the fitting parameters and they are respectively equal to 164.2 GPa and 6.24. It is noticeable that the value of N_C obtained by fitting the experimental data is very close of the mean coordination number N_C deduced from the microstructure observation of the dense β-TCP ceramic. Indeed, the mean coordinate number, calculated on 520 grains by image analysis with Image Pro Plus©software from Media Cybernetics grains, is equal to 6 as shown as an example in Fig. 5.

In addition, the value of E_0 deduced from the application of the model is very close to that measured on the dense ceramic, i.e. 165.9 GPa. These results on the elastic modulus and the coordinate number validate the model representing the influence of the porosity on the elastic modulus of β-TCP microporous ceramics. Nevertheless, this model is only validated for porosity volume fraction ranging between 0% and 14%. Then, it should be extended for β-TCP microporous and/or macroporous ceramics including higher porosity density.

4.2. Hardness

To represent the hardness-load dependence, the square of the hardness number is plotted as a function of the inverse of the maximum indentation depth according to relation (11). In order

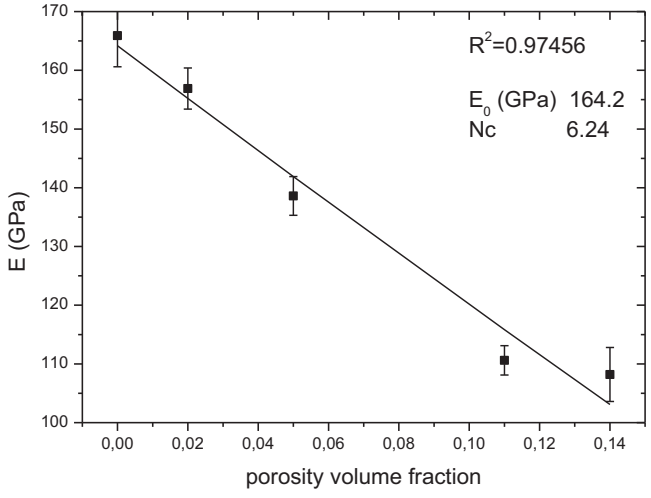

Fig. 4. Elastic modulus variation as a function of the porosity volume fraction for the β-TCP microporous ceramics.

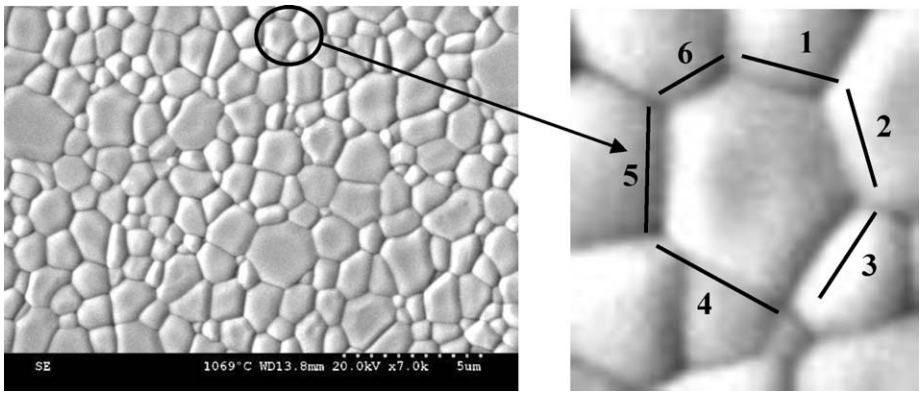

Fig. 5. SEM micrograph of the dense β-TCP ceramic illustrating that the mean coordinate number is equal to 6.

to compare Vickers and Martens hardness, we represented the two hardness numbers. As an example, Fig. 6 represents the two hardness numbers variations observed for the dense β-TCP ceramic. This figure clearly shows that relation (11) adequately represents the hardness-load dependence but the variations are quite distinct for the two hardness numbers.

The same result is also observed for the microporous β-TCP ceramics. Then we collected in Table 4 the macrohardness and the hardness length-scale factor deduced respectively from the intercept of the straight line with the y-axis and from the square root of the slope. Analysis of the results leads to several conclusions. By studying the correlation factors, R^2, collected in Table 4, it is noticeable that the errors obtained for Vickers hardness measurements are higher than the errors obtained for Martens hardness measurements. Obviously, the values of R^2 obtained on Vickers hardness, around 0.5, would render inaccurate the related analysis. To explain such a difference, Shahdad et al.[34] compared Vickers and Martens hardness measurements of dental materials and showed that the accuracy of the Vickers measurements could not be guaranteed due to the presence of cracks visible along the indent diagonals. This indicates the magnitude of error that can be encountered when measuring hardness of materials using traditional hardness tests requiring the indent diagonals measurement. Moreover, Martens hardness calculation allows eliminating subjective bias. The lowest standard deviations indicate a good reproducibility and a correct accuracy of the instrumented indentation test. Fig. 7 shows the cracks along the indent diagonals and delamination close to the edge both leading to an inaccurate measurement of the diagonal length.

Thereafter, we propose studying the Martens hardness and analysing the evolution of the macrohardness, HM_0, and the hardness length-scale factor, H_{LSF}, as a function of the porosity volume fraction, p. Fig. 8 represents these two parameters deduced from Martens hardness calculation as a function of p.

By studying β-TCP ceramics, Tancret et al.[33] suggested to extend Eq. (12) for modelling the hardness variation as a function of the porosity. The authors based their assumptions on the fact that the evolution of the elastic modulus and the toughness with the porosity are equivalent when the fracture mechanism remains the same independently on the porosity rate. In addition, they assume that, during indentation, the ceramics deform mainly by micro-cracking between macro-pores. They add that deformation mechanism under the indenter is equivalent to a fracture mechanism. By applying this model, we found a coordi-

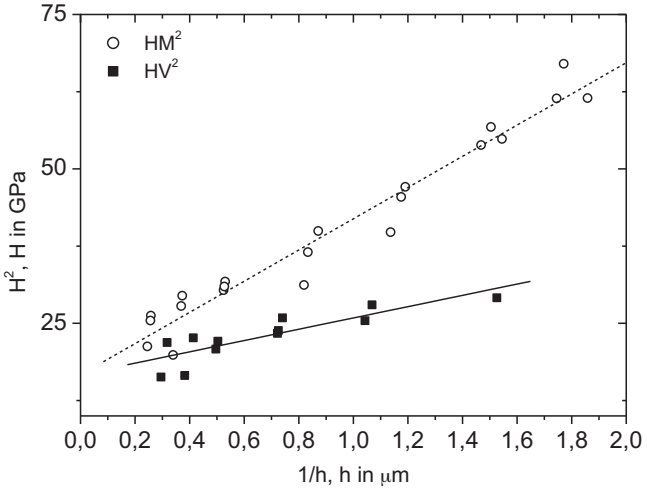

Fig. 6. Representation of the square of the hardness as a function of the inverse of the maximum indentation depth according to the relation (11) following Vickers and Martens hardness calculation for the dense β-TCP ceramic.

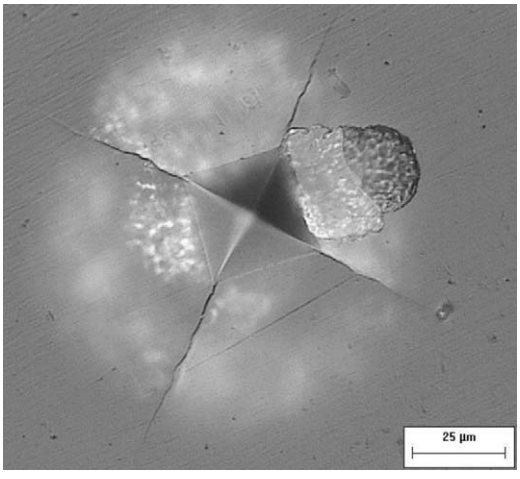

Fig. 7. Cracks along the diagonals and delamination close to the edge of the indent ($P = 5$ N) performed on the dense β-TCP ceramic with a Vickers indenter.

Table 4
Macrohardness and hardness length-scale factor calculated for Vickers and Martens hardness as a function of the porosity of the β-TCP ceramics.

Density	Vickers hardness			Martens hardness		
	H_0 (GPa)	H_{LSF} (MPa m$^{1/2}$)	R^2	H_0 (GPa)	H_{LSF} (MPa m$^{1/2}$)	R^2
86%	2.50 ± 0.13	1.04 ± 0.19	0.494	2.41 ± 0.08	2.57 ± 0.10	0.944
89%	2.54 ± 0.17	1.47 ± 0.13	0.797	2.23 ± 0.20	3.11 ± 0.18	0.884
95%	3.59 ± 0.27	2.15 ± 0.49	0.514	3.53 ± 0.10	3.90 ± 0.10	0.976
98%	4.26 ± 0.17	1.37 ± 0.25	0.505	4.25 ± 0.15	4.58 ± 0.14	0.966
100%	4.09 ± 0.16	3.02 ± 0.28	0.858	4.31 ± 0.17	4.97 ± 0.13	0.973

nate number close to 9 which has no significant meaning. On the other hand, Tancret et al.[33] found a coordinate number equals to 3 by indenting with a ball indenter. They explained the difference between the calculated and the theoretical values of N_C (between 5 and 7) by the very high micro-porosities (up to 62%) and by the fracture mechanisms of their ceramics. In fact, the authors used different applied loads depending on the hardness of the material. That is why the authors would have take into account the indentation size effect. In addition, to modify the model of Jernot et al.,[32] the authors considered that the deformation under the indenter mainly results from ceramic fracture between macropores. But, for microporous ceramics, the deformation probably comes from plastic deformation and/or intergranular or transgranular fractures. Moreover, in highly porous materials, the porosity filling under the indenter is a mechanism which should not be neglected to explain the hardness decrease.[35] In order to circumvent such a discussion, we prefer describing the hardness behaviour by using linear regression of the experimental data.

Indeed, Fig. 8 shows that a linear relation allows adequately representing both the macrohardness and the hardness length-scale factor as a function of the porosity volume fraction. It is clearly seen that these two parameters decrease when the porosity volume fraction increases as it was expected. The two corresponding relations are:

$$\begin{cases} \mathrm{HM}_0 = 4.3 - 14.2p \\ \mathrm{HM}_{LSF} = 4.9 - 16.6p \end{cases} \quad (13)$$

where 4.3 GPa and 4.9 MPa m$^{1/2}$ correspond to the values of the parameters HM_0 and HM_{LSF} for the dense β-TCP ceramic respectively.

It is noticeable that the relative variation of the two parameters, i.e. the macrohardness and the hardness length-scale factor, can be expressed as a function of p by using almost the same relation:

$$\frac{\mathrm{HM}_0 - \mathrm{HM}_{0_{dense}}}{\mathrm{HM}_{0_{dense}}} = -3.30p \quad (14)$$

and

$$\frac{\mathrm{HM}_{LSF} - \mathrm{HM}_{LSF_{dense}}}{\mathrm{HM}_{LSF_{dense}}} = -3.39p \quad (15)$$

This result is very interesting since it confirms that the hardness length-scale factor can be used as an indicator of the plastic deformation under the indent as well as the macrohardness for characterizing the plastic deformation resistance by indentation. In addition, Fig. 4 shows also a linear representation of the elastic modulus as a function of the porosity volume fraction. This indicates that the relative variation of the elastic modulus must follow the same tendency. Therefore, we represented in Fig. 9 the relative variations of E, HM_0 and HM_{LSF} on the same graph as a function of the porosity volume fraction. Depending on the standard deviation, it is nevertheless remarkable that these three different parameters can be expressed as a function of the porosity with an equivalent relation as Eq. (14). In a first approxi-

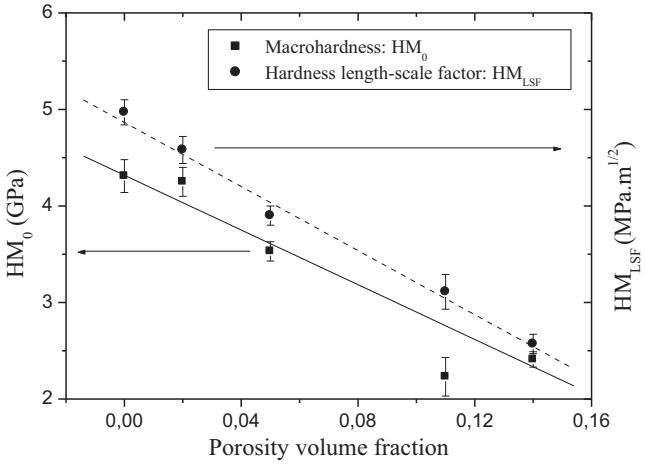

Fig. 8. Macrohardness and hardness length-scale factor from Martens hardness variation as a function of the porosity volume fraction.

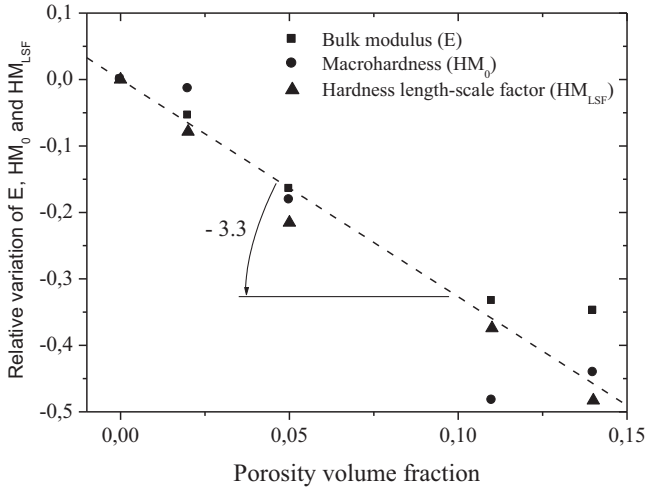

Fig. 9. Relative variation of the elastic modulus, the macrohardness and the hardness length-scale factor as a function of the porosity volume fraction.

mation, the ratio between the relative variation of the mechanical properties and the porosity volume fraction is close to $N_C/2$. Nevertheless, additional studies must be performed for validating such a definition and/or for connecting the proportionality factor to an intrinsic property of the material.

5. Conclusions

To study the influence of the microporosity of β-TCP ceramic, instrumented indentation test is preferred since the cracks generated around the residual indents impede suitable diagonal measurements by usual Vickers indentation tests. In addition, in the range of porosity studied here (0–14%), the elastic modulus and the hardness follow the same tendency, i.e. the mechanical properties decrease when the porosity increases as it was expected by the theory. However, it is noticeable that the indentation size effect, based on the study of the hardness length-scale factor derived from the strain gradient plasticity theory is in the same manner affected by the porosity. And finally, we observed that the relative variation of the elastic modulus, the macrohardness and the hardness length-scale factor can be expressed by the same mathematical relation as a function of the porosity volume fraction.

References

1. Burg KJL, Porter S, Kellam JF. Biomaterial developments for bone tissue engineering. *Biomaterials* 2000;**21**(23):2347–59.
2. Jarcho M. Calcium phosphate ceramics as hard tissue prosthetics. *Clinical Orthopaedics and Related Research* 1981;**157**:259–78.
3. Hench LL. Bioceramics. *Journal of the American Ceramic Society* 1998;**81**:1705–28.
4. Engin NO, Tas AC. Manufacture of macroporous calcium hydroxyapatite bioceramics. *Journal of the European Ceramic Society* 1999;**19**:2569–72.
5. Xie Y. Biomatériaux hybrides innovants et leur évaluation in vivo. PhD Thesis. Université du Littoral Côte d'Opale, Boulogne, France; 2006.
6. Ginebra MP, Traykova T, Planell JA. Calcium phosphate cements as bone drug delivery systems: a review. *Journal of Controlled Release* 2006;**113**(2):102–10.
7. Rauschmanna MA, Wichelhausb TA, Stirnalc V, Dingeldeinc E, Zichnera L, Schnettlerd R, et al. Nanocrystalline hydroxyapatite and calcium sulphate as biodegradable composite carrier material for local delivery of antibiotics in bone infections. *Biomaterials* 2005;**26**:2677–84.
8. Hornez JC, Chai F, Blanchemain N, Lefèvre A, Descamps M, Hildebrand HF. Biocompatibility improvement of pure hydroxyapatite (HA) with different porosity. Proceedings of "Bioceramics19", Chengdu, PR China; 2006. Key Engineering Materials 2007;330–332:927–30.
9. Bowers KT, Keller JC, Randolph BA, Wick DG, Mickaels CM. Optimization of surface micromorphology for enhanced osteoblast responses in vitro. *International Journal of Oral and Maxillofacial Implants* 1992;**7**:302–10.
10. LeGeros RZ, Parsons JR, Daculsi G, Driessens F, Lee D, Liu ST, et al. Significance of the porosity and physical chemistry of calcium phosphate ceramics. Biodegradation–bioresorption. *Annals of the New York Academy of Sciences* 1988;**523**:268–71.
11. Malzbender J, den Toonder JMJ, Balkenende AR, de With G. Measuring mechanical properties of coatings: a methodology applied to nano-particle-filled sol–gel coatings on glass. *Materials Science and Engineering R: Reports* 2002;**36**(2–3):47–103.
12. Wang CX, Zhou X, Wang M. Influence of sintering temperatures on hardness and Young's modulus of tricalcium phosphate bioceramic by nanoindentation technique. *Materials Characterisation* 2004;**52**:301–7.
13. Saber-Samandari S, Gross KA. Micromechanical properties of single crystal hydroxyapatite by nanoindentation. *Acta Biomaterialia* 2009;**5**:2206–12.
14. Viswanath B, Raghavan R, Gurao NP, Ramamurty U, Ravishankar N. Mechanical properties of tricalcium phosphate single crystals grown by molten salt synthesis. *Acta Biomaterialia* 2008;**4**:1448–54.
15. Tang CY, Uskokovic PS, Tsui CP, Veljovic Dj, Petrovic R, Janackovic Dj. Influence of microstructure and phase composition on the nanoindentation characterization of bioceramic materials based on hydroxyapatite. *Ceramics International* 2009;**35**:2171–8.
16. Chicot D. Hardness length-scale factor to model nano- and micro-indentation size effects. *Materials Science and Engineering A* 2009;**499**(1–2):454–61.
17. Descamps M, Hornez JC, Leriche A. Effects of powder stoichiometry on the sintering of β-tricalcium phosphate. *Journal of the European Ceramic Society* 2007;**27**:2401–6.
18. Oliver WC, Pharr GM. An improved technique for determining hardness and elastic modulus using load and displacement sensing indentation experiments. *Journal of Materials Research* 1992;**7**(6):1564–83.
19. Sneddon IN. Boussiness's problem for a rigid cone. *Proceedings of the Cambridge Philosophical Society* 1948;**44**:492–507.
20. King RB. Elastic analysis of some punch problems for layered medium. *International Journal of Solids and Structures* 1987;**23**(12):1657–64.
21. Dao M, Chollacoop N, Van Vliet KJ, Venkatesh TA, Suresh S. Computational modeling of the forward reverse problems in instrumented sharp indentation. *Acta Materialia* 2001;**49**(19):3899–918.
22. Antunes JM, Menezes LF, Fernandes JV. Three-dimensional numerical simulation of Vickers indentation tests. *International Journal of Solids and Structures* 2006;**43**(3–4):784–806.
23. Hay JC, Bolshakov A, Pharr GM. Critical examination of the fundamental relations used in the analysis of nano-indentation data. *Journal of Materials Research* 1999;**14**(6):2296–305.
24. Chicot D, Roudet F, Lepingle V, Louis G. Strain gradient plasticity to study hardness behaviour of magnetite (Fe_3O_4) under multicycles indentation. *Journal of Materials Research* 2009;**24**(3):749–59.
25. Fischer-Cripps AC. Critical review of analysis and interpretation of nanoindentation test data. *Surface and Coatings Technology* 2006;**200**(14):4153–65.
26. Cheng YT, Cheng CM. Scaling, dimensional analysis, and indentation measurements. *Materials Science and Engineering R: Reports* 2004;**44**(4–5):91–149.
27. Gong J, Wu J, Guan Z. Examination of the indentation size effect in low-load Vickers hardness testing of ceramics. *Journal of the European Ceramic Society* 1999;**19**:2625–31.
28. Peng Z, Gong J, Miao H. On the description of the indentation size effect in hardness testing for ceramics: analysis of the nanoindentation data. *Journal of the European Ceramic Society* 2004;**24**:2193–201.
29. Chicot D, Roudet F, Soom A, Lesage J. Interpretation of instrumented hardness measurements on stainless steel with different surface preparations. *Surface Engineering* 2007;**23**(1):32–9.
30. Nix WD, Gao H. Indentation size effects in crystalline materials: a law for strain gradient plasticity. *Journal of the Mechanics and Physics of Solids* 1998;**46**(3):411–25.
31. Field JE, Telling RH. The Young modulus and Poisson ratio of diamond. Research Note, Cavendish Laboratory, Cambridge; 1999.
32. Jernot JP, Coster M, Chermant JL. Model to describe the elastic modulus of sintered materials. *Physica Status Solidi (a)* 1982;**72**(1): 325–32.
33. Tancret F, Bouler JM, Chamousset J, Minois LM. Modelling the mechanical properties of microporous and macroporous biphasic calcium phosphate bioceramics. *Journal of the European Ceramic Society* 2006;**26**(16):3647–56.
34. Shahdad SA, McCabe JF, Bull S, Rusby S, Wassell RW. Hardness measured with traditional Vickers and Martens hardness methods. *Dental Materials* 2007;**23**(9):1079–85.
35. Luo J, Stephens R. Porosity-dependence of elastic moduli and hardness of 3Y-TZP ceramics. *Ceramics International* 1999;**25**: 281–6.